HHS Public Access

Author manuscript

J Cell Physiol. Author manuscript; available in PMC 2020 August 14.

Published in final edited form as:

J Cell Physiol. 2019 September ; 234(9): 16376–16388. doi:10.1002/jcp.28306.

The Apical Na^+-HCO_3^- Cotransporter Slc4a7 (NBCn1) does not contribute to Bicarbonate Transport by Mouse Salivary Gland Ducts

Ning-Yan Yang[1,2], **Taro Mukaibo**[1,3], **Ira Kurtz**[4], **James E. Melvin**[1]

[1]Secretory Mechanisms and Dysfunctions Section, National Institute of Dental and Craniofacial Research, National Institutes of Health, Bethesda, MD, 20892, USA

[2]Department of Pediatric Dentistry, Beijing Stomatological Hospital & School of Stomatology, Capital Medical University, Beijing, 100050, China

[3]Department of Oral Reconstruction and Rehabilitation, Kyushu Dental University, Kitakyushu, Fukuoka, 803-8580, Japan

[4]Department of Medicine, Division of Nephrology, David Geffen School of Medicine, and the Brain Research Institute, University of California, Los Angeles, CA, 90095, USA

Abstract

The HCO_3^- secretion mechanism in salivary glands is unclear but is thought to rely on the coordinated activity of multiple ion transport proteins including members of the *Slc4* family of bicarbonate transporters. Slc4a7 immunolocalized to the apical membrane of mouse submandibular duct cells. In contrast, Slc4a7 was not detected in acinar cells, and correspondingly, *Slc4a7* disruption did not affect fluid secretion in response to cholinergic or β-adrenergic stimulation in the submandibular gland. Much of the Na^+-dependent intracellular pH regulation in submandibular gland duct cells was insensitive to DIDS, S0859 and to removal of extracellular HCO_3^-. Consistent with these latter observations, the *Slc4a7* null mutation had no impact on HCO_3^- secretion nor on intracellular pH regulation in duct cells. Taken together, our results revealed that Slc4a7 targets to the apical membrane of mouse submandibular gland duct cells where it contributes little if any to intracellular pH regulation or stimulated HCO_3^- secretion.

Abbreviated Abstract

Mouse Slc4a7 is a DIDS and S0859 sensitive Na^+-HCO_3^- cotransporter that is expressed in the apical membrane of mouse submandibular duct cells but not acinar cells. *Slc4a7* disruption did not affect fluid secretion by the mouse submandibular gland nor does Slc4a7 contribute to intracellular pH regulation or stimulated HCO_3^- secretion.

Correspondence James E. Melvin, D.D.S., Ph.D. Secretory Mechanisms and Dysfunctions Section, National Institute of Dental and Craniofacial Research, National Institutes of Health, Bethesda, MD, 20892, USA. james.melvin@nih.gov.

AUTHOR CONTRIBUTIONS

N.Y.Y., T.M., I.K. and J.E.M. conceived and designed the research; N.Y.Y., and T.M. performed research; N.Y.Y., T.M., and J.E.M. analyzed and interpreted data; N.Y.Y., T.M., and J.E.M. drafted the manuscript; and N.Y.Y., T.M., I.K. and J.E.M. edited, revised and approved the final version of manuscript.

CONFLICTS OF INTEREST

No conflicts of interest, financial or otherwise, are declared by the authors.

Keywords

Bicarbonate; Cotransporter; Fluid secretion; Submandibular gland; Slc4a7

1 INTRODUCTION

The *SLC4* gene family consists of 10 members (SLC4A1–5, SLC4A7–11), nine of which fall into three major groups of HCO_3^- transporters: Cl^--HCO_3^- exchangers, Na^+-HCO_3^- cotransporters and Na^+-driven Cl^-/HCO_3^- exchanger (Pena-Munzenmayer, George, Shull, Melvin, & Catalan, 2016; Romero, Chen, Parker, & Boron, 2013). With the exception of SLC4A11, which does not transport HCO_3^- (Kao et al., 2016; Myers, Marshall, Jennings, & Parker, 2016; Vilas et al., 2013), SLC4 ion transport proteins mediate transmembrane HCO_3^- flux to regulate intracellular pH (Choi, 2012; Parker, 2018). The *Slc4* family members that exchange Cl^- and HCO_3^- have been proposed to contribute to salivary gland HCO_3^- and/or fluid secretion (Ishiguro, Steward, Lindsay, & Case, 1996; Luo et al., 2001; Nguyen, Stuart-Tilley, Alper, & Melvin, 2004; Park et al., 2002). Slc4a2 (Ae2) and Slc4a9 (Ae4) promote Cl^--HCO_3^- exchange in the secretory acinar cells, but only mice deficient in the cation-driven Cl^--HCO_3^- exchanger Slc4a9 secrete less saliva (Pena-Munzenmayer et al., 2015; Vera-Siguenza, Catalan, Pena-Munzenmayer, Melvin, & Sneyd, 2018). There is little direct evidence to support the speculation (Ishiguro et al., 1996; Luo et al., 2001; Park et al., 2002) that the Slc4a Na^+-HCO_3^- cotransporters (NBC) are involved in HCO_3^- and/or fluid secretion in salivary gland.

SLC4A7 (NBCn1, also known as NBC3) was first cloned from human skeletal muscle cells (Pushkin et al., 1999). Rat Slc4a7 is an electroneutral Na^+-HCO_3^- cotransporter that operates with a stoichiometry of 1 Na^+ to 1 HCO_3^- (Choi, Aalkjaer, Boulpaep, & Boron, 2000). Slc4a7 has a wide tissue distribution, including skeletal muscle, smooth muscle, heart, kidney, epididymis, cornea, and salivary gland (Boedtkjer, Praetorius, Fuchtbauer, & Aalkjaer, 2008; Choi et al., 2000; Damkier, Nielsen, & Praetorius, 2006; Kwon, Pushkin, Abuladze, Nielsen, & Kurtz, 2000; Luo et al., 2001; Pushkin et al., 1999; Pushkin, Clark, Kwon, Nielsen, & Kurtz, 2000; Shei, Liu, Htoon, Aung, & Vithana, 2013). It has been proposed that Slc4a7 plays an important role in intracellular pH regulation (Boedtkjer & Aalkjaer, 2012; Boedtkjer, Bentzon, Dam, & Aalkjaer, 2016; Boedtkjer, Praetorius, & Aalkjaer, 2006), hypertension development (Boedtkjer et al., 2011; Lu et al., 2015; L. Wang et al., 2017) and increased breast cancer risk (Gorbatenko, Olesen, Boedtkjer, & Pedersen, 2014). Of note, *Slc4a7*$^{-/-}$ mice develop blindness and auditory impairment (Bok et al., 2003).

The concentration of HCO_3^- in saliva is receptor agonist and flow rate dependent (Lau, Howorth, & Case, 1990; Young, Cook, Evans, & Pirani, 1987; Young, Martin, Asz, & Weber, 1970), however the underlying HCO_3^- transport mechanism remains unclear. HCO_3^- secretion in exocrine salivary glands is thought to rely on the coordinated activity of multiple ion transport proteins expressed in the apical membranes of duct cells including the cystic fibrosis transmembrane conductance regulator (Cftr) channel and bicarbonate transporting members of the *Slc26* and *Slc4* families (Gresz et al., 2002; Hong, Park, Shcheynikov, &

Muallem, 2014; Park et al., 2002). However, it was recently demonstrated that Slc26a6 primarily targets to the apical membrane of acinar cells where it does not appear to be involved in HCO_3^- secretion (Mukaibo, Munemasa, George, et al., 2018). Slc4a7 was detected in guinea pig and mouse salivary gland acinar and duct cells (Li et al., 2006; Luo et al., 2001), but its involvement in HCO_3^- secretion was not explored.

The goal of the present study was to take advantage of the *Slc4a7* null mouse to test the hypothesis that the Na^+-HCO_3^- cotransporter Slc4a7 plays a major role in HCO_3^- secretion by the submandibular gland (SMG). In contrast to human SLC4A7 (Pushkin et al., 1999) and rat Slc4a7 (Choi et al., 2000), we found that mouse Slc4a7 mediates Na^+-HCO_3^- cotransport activity that is fully blocked by DIDS (4,4'-Diisothiocyano-2,2'-stilbenedisulfonic acid). Thus, the functional properties of Slc4a7 appear to be species-specific, and moreover, our results demonstrate that Slc4a7 exclusively targets to the apical membrane of SMG duct cells where it appears to contribute little if any to the secretion of saliva or HCO_3^- transport.

2 MATERIALS AND METHODS

2.1 Animals

Slc4a7$^{-/-}$ and *Slc4a7*$^{+/+}$ littermate mice (129-Sv/Ev^{Brd} background) were generated as previously described (Bok et al., 2003). Genotyping was performed using the following PCR primers: forward primer (5'-GGTGGTGACCGATGGAGTAA-3') from the deleted region and a reverse primer (5'-CTTCAAATCTGGCTTGTTGGC-3') of *Slc4a7*; and (5'-GTGTGGCGGACCGCTATCA −3') a forward primer at the 5' end of the selection cassette. Mice were housed in micro-isolator cages with *ad libitum* access to laboratory chow and water with a 12-h light/dark cycle. Experiments were performed on 10–13 weeks old female and male *Slc4a7*$^{+/+}$ and *Slc4a7*$^{-/-}$ littermate animals. *Slc4a7*$^{-/-}$ mice grew and developed normally such that the body weights were not significantly different from age and sex matched *Slc4a7*$^{+/+}$ mice (Table 1), confirming that systemic disruption of *Slc4a7* has little impact on the general development or health (Bok et al., 2003). Moreover, the morphology of the SMG of female and male *Slc4a7*$^{-/-}$ mice appeared to be grossly normal with no change in gland weight (Table 1) nor in the percent of acinar cells (Figure 1). Note that the ductal to acinar ratios for the submandibular glands of the male and female 129-Sv/Ev^{Brd} mice used in the present study (male *Slc4a7*$^{-/-}$ and *Slc4a7*$^{+/+}$ = 1.11±0.05 and 1.24±0.05, respectively; female *Slc4a7*$^{-/-}$ and *Slc4a7*$^{+/+}$ = 0.29±0.01 and 0.30±0.01, respectively) were comparable to the ductal to acinar ratios previously reported for male and female C57BL/6J A^{w-J}-Ta^{6J} mice (Mukaibo, Munemasa, Masaki, Cui, & Melvin, 2018). All animal procedures were approved by the National Institute of Dental and Craniofacial Research, National Institutes of Health, Animal Care and Use Committee (ASP 16–802).

2.2 Solutions

The composition of solutions used for *ex vivo* perfusion and intracellular pH measurements are given in Table 2 (Solutions A-I). The osmolality of solutions was measured by a freezing-point depression osmometer (Advanced Instruments, Norwood, MA) and adjusted

to 300 mOsm/kg with sucrose. All reagents were from Sigma-Aldrich unless otherwise indicated.

2.3 Immunofluorescence and histology

Five μm thick sections of paraformaldehyde fixed mouse SMG were deparaffinized and antigen retrieval was performed as described previously (Mukaibo, Munemasa, George, et al., 2018). Sections were blocked in 1% BSA in PBS (phosphate buffered saline) for 30 min at RT, and then incubated at 4°C with rabbit anti-Slc4a7 (1:100 dilution, OriGene, Cat# TA322834, RRID: AB_2749851) and goat anti-Slc12a2 (NKCCl, 1:100 dilution, Santa Cruz Biotechnology, Cat# sc-21545, RRID: AB_2188633) antibodies overnight. The anti-Slc4a7 antibody recognizes the C-terminus sequence "DEPSKKYMDAETSL" of all mouse Slc4a7 variants (Liu, Yang, & Chen, 2015). Samples were washed with PBS and then incubated for 60 min at RT with donkey anti-rabbit Alexa Fluor 594 (1:200 dilution, Jackson ImmunoResearch Labs, Cat# 711–587-003, RRID: AB_2340623) and donkey anti-goat Alexa Fluor 488 (1:400 dilution, Jackson ImmunoResearch Labs, Cat# 705–546-147, RRID: AB_2340430) secondary antibodies. Slides were mounted using Fluoroshield™ with DAPI (Sigma-Aldrich, St. Louis, MO) and visualized on a confocal Olympus Fluoview microscope at 40× magnification. Additional sections were stained with hematoxylin-eosin (HE) and images captured with a DS-Fit1 Nikon camera mounted on a Nikon Eclipse 50i microscope and Leica Aperio CS2 20x objective. The ductal cross-sectional area was calculated using Image-J software (https://imagej.nih.gov/ij/), and the acinar cross-sectional area subsequently was estimated as previously described by subtracting the duct cross-sectional area from the stromal-omitted, gland cross-sectional area (Mukaibo, Munemasa, Masaki, et al., 2018). Given that salivary gland fluid is generated by acinar cells, the % of the gland mass reflecting the secretory acinar compartment was used to normalize function (see Table 1).

2.4 *Ex vivo* mouse submandibular gland (SMG) perfusion

Ex vivo SMG perfusion was performed as reported previously with minor modifications (Pena-Munzenmayer et al., 2015). Briefly, mice were anesthetized with chloryl hydrate (400mg/kg, intraperitoneal injection). Following ligation of all branches of the common carotid artery except the submandibular artery, the gland was transferred to a perfusion chamber where the common carotid was cannulated (31-gauge) and perfused at 37°C with a physiological HCO_3^- containing, high Cl^- solution (Solution A, Table 2). The submandibular duct was inserted into a capillary tube and saliva was induced using one of the following two stimulation protocols: (1) Figure 3. 20 min stimulation with the β-adrenergic receptor agonist isoproterenol (IPR; 1.0 μM), a 15 min washout period, followed by 10 min perfusion with the cholinergic receptor agonist carbachol (CCh; 0.3 μM); or (2) Figure 4. 10 min stimulation with 1.0 μM IPR plus 0.3 μM CCh. Progression of saliva within the capillary tube was recorded every minute. Regardless of the agonist used male submandibular glands secreted more saliva than female glands, consistent with the larger size of the male gland. A summary of the amount of saliva secreted in response to different agonists is given separately for male and female glands in Table 1 (saliva amounts normalized to % acinar area are also given in brackets). Of note, disruption of *Slc4a7* had no significant impact on the amount of saliva secreted by the submandibular glands of either sex. Consequently,

Figures 3 and 4 display pooled results from male and female glands. The collected saliva was stored at −20°C until analysis.

2.5 Ion concentration measurement

The HCO_3^- concentration of saliva was assayed according to the manufacturer's instructions (Carbon Dioxide Enzymatic Assay kit, Cat# DZ122A-K, Diazyme Laboratories, Poway, CA). Sodium and potassium concentrations were analyzed by atomic absorption spectroscopy (PerkinElmer Life Sciences 3030 spectrophotometer, PerkinElmer, Boston, MA). Chloride activity was measured using a digital expandable ion analyzer EA940 (Orion Research, Edison, NJ). The magnitude of Na^+ and Cl^- reabsorption was estimated as previously described (Mukaibo, Munemasa, Masaki, et al., 2018). In brief, the Na^+ and Cl^- concentrations of the final SMG ductal saliva measured in the present study were subtracted from the previously reported Na^+ and Cl^- concentrations (157.2 and 122.9 mM, respectively) for the primary saliva collected from male mouse SMG acinar cells (Mangos, McSherry, Nousia-Arvanitakis, & Irwin, 1973).

2.6 Cell culture and transfections

CHO-K1 cells (ECACC, Cat# 85050302, RRID: CVCL_0213) were grown in F12 medium (Thermo Fisher Scientific, Waltham, MA) containing 10% (vol/vol) fetal bovine serum (Thermo Fisher Scientific) and 1% penicillin-streptomycin (10000 U/ml; Thermo Fisher Scientific). Plasmids encoding Mus *Slc4a7* (Gene Bank accession no. NM_001033270), the empty pCMV6-Entry vector control and human CD8A (Gene Bank accession no. NM_001768) were obtained from OriGene (Rockville, MD). Cells were electroporated (Nucleofector II, Amaxa, Nordrhein-Westfalen, Germany) with equal amounts of plasmid DNA (6 μg for each plasmid) using Nucleofector kit V (Lonza, Allendale, NJ) according to the manufacturer's instruction and seeded onto 5-mm-diameter coverslips (Warner Instrument, Hamden, CT). Intracellular pH (pH_i) measurements were performed 18–20 hr after electroporation.

2.7 SMG duct cell isolation

Ducts were isolated from SMG using a previously described procedure (Yang et al., 2017) with minor modifications to preserve ductal structure. Briefly, mice were euthanized by CO_2 asphyxiation followed by cervical dislocation. SMG from *Slc4a7*$^{-/-}$ and *Slc4a7*$^{+/+}$ mice were dissected and minced prior to digestion for 20 min with Liberase™ TL (0.125 mg/ml; Roche, Indianapolis, IN) in Eagle's minimum essential medium (MEM; Corning, Corning, NY) solution containing 1% BSA (Sigma-Aldrich). After digestion, the cell pellet was passed through a Pierce™ Tissue Strainer (250 μm, Thermo Fisher Scientific) and resuspended in MEM. Under these isolation conditions intact ducts appear on the stage of the microscope as elongated linear structures and are easily differentiated from the spherical acini. All solutions were gassed continuously with 95% O_2/5% CO_2 and maintained at 37°C.

2.8 Intracellular pH measurement

SMG cells were loaded with the pH indicator BCECF by incubation with 4 μM BCECF-AM (2',7 -bis-(2-carboxyethyl)-5-(and-6)-carboxyfluorescein, acetoxymethyl ester, Thermo

Fisher Scientific) in MEM for 30 min, and then the Na^+ dependent intracellular pH (pH_i) recovery monitored following an NH_4^+-prepulse induced intracellular acidosis. Transfected CHO-K1 cells were incubated for 30 min with 2 μM BCECF-AM and Dynabeads™ CD8 beads (1:500, Thermo Fisher Scientific) in K^+ free solution (Solution B, Table 2) containing 0.1 mM of the Na^+-K^+ ATPase inhibitor Ouabain (Sigma-Aldrich). Extracellular Na^+ was removed for at least 5 min, and then the intracellular alkalinization monitored following re-addition of extracellular Na^+. Mus *Slc4a7* or empty pCMV6-Entry vector control plasmid was co-transfected with human CD8A plasmid, and the intracellular pH monitored in CD8 positive cells decorated with beads. Imaging experiments were performed using an inverted microscope (IX71; Olympus, Center Valley, PA) equipped with an OptoScan monochromator system (Cairn Research, Kent, UK) coupled to a high-speed digital camera (C11440; Hamamatsu, Tokyo, Japan). Images of BCECF fluorescence were acquired by alternate excitation at 490 and 440 nm, and emissions captured at 530 nm using Imaging WorkBench 6.0 software (INDEC BioSystems, http://www.indecbiosystems.com/imagingworkbench/default.asp, RRID: SCR_016589). All solutions were kept at 37°C using a CL-100 bipolar temperature controller (Warner Instruments).

2.9 Quantitative polymerase chain reaction (qPCR)

qPCR was performed as previously described (Mukaibo, Munemasa, George, et al., 2018). Briefly, SMG were immediately frozen in liquid nitrogen and shipped to MyOmicsDx (Towson, MD) for processing. Total RNA was isolated, and reverse transcribed to synthesize cDNA. Real-Time PCR was performed to determine the mRNA levels for members of the *Slc4* gene family (*a2, a4, a5, a8, a9, a10* and *a11*), Na^+/H^+ exchangers *Slc9* (*a1, a2* and *a3*) and the *Cftr* anion channel using Bio-Rad CFX96 Touch™ Real-Time PCR Detection System with specific primer pairs (Table 3). mRNA levels were normalized to the abundance of *β-actin* message.

2.10 Statistical analysis

Results are presented as the mean ± SEM showing values for individual mice ($n \geq 6$) or CHO-K1 cells ($n \geq 10$ transfections). Statistical significance was determined using the Student's *t* test. Multiple-sample comparisons were performed using one-way ANOVA followed by Bonferroni's *post hoc* test. A p value <0.05 was considered statistically significant. Origin 8.0 software (Origin, http://www.originlab.com/index.aspx?go=PRODUCTS/Origin, RRID: SCR_014212) was used for statistical calculations.

3 RESULTS

3.1 Slc4a7 targets to the apical membrane of SMG duct cells

The cellular distribution of the Na^+-HCO_3^- cotransporter Slc4a7 was examined in mouse SMG by immunofluorescence. Slc4a7 primarily localized to the apical membrane of SMG duct cells with faint intracellular staining in *Slc4a7*$^{+/+}$ mice (Figures 2a, c, green stain, white arrowheads). In contrast, no Slc4a7-positive staining was detected in acinar cell, while an antibody against the Na^+-K^+-Cl^- cotransporter Slc12a2 (Nkcc1) specifically labelled the basolateral membrane of acinar cells of wildtype mice (Figures 2b, c, e and f, red stain, yellow arrows). No apical or intracellular Slc4a7 immunostaining was detected in the

SMG ducts of *Slc4a7* $^{-/-}$ mice (Figures 2d, f), confirming the specificity of the C-terminal-directed Slc4a7 primary antibody. Basolateral immunostaining of Slc12a2 was not affected in the SMG of *Slc4a7* null mouse (Figures 2e, f).

3.2 *Slc4a7* disruption fails to change the kinetics or magnitude of stimulated fluid secretion in the SMG

Acinar cells account for most of the fluid secretion in salivary glands (Lee, Ohana, Park, Yang, & Muallem, 2012; Melvin, Yule, Shuttleworth, & Begenisich, 2005). Thus, given that Slc4a7 was not detected in SMG acinar cells (Figure 2), we predicted that Slc4a7 would not be involved in fluid secretion. Of note, salivary glands are innervated by both the parasympathetic cholinergic and sympathetic adrenergic systems (Proctor, 2016). Consequently, we tested whether the kinetics and the amount of fluid secretion in *Slc4a7*$^{-/-}$ and *Slc4a7*$^{+/+}$ mice were influenced either by β-adrenergic receptor agonist isoproterenol (IPR) or by cholinergic receptor agonist carbachol (CCh) stimulation. *Ex vivo* perfusion with IPR followed by CCh (after 15 min washout) revealed that the flow rate of SMG was nearly 10-fold greater in response to the cholinergic receptor agonist than to the β-adrenergic receptor agonist in both wildtype and *Slc4a7*$^{-/-}$ mice (Figure 3a, note break in Y axis). Figure 3a also shows that there were no apparent differences in the kinetics, i.e. the time required to reach the maximum secretion rate was unchanged (≤1 minute in all cases) and the sustained secretion rate was relatively constant throughout stimulation. Consequently, the total amount of saliva secretion was unaffected in the SMG of *Slc4a7*$^{+/+}$ and *Slc4a7*$^{-/-}$ mice in response to either β-adrenergic or cholinergic receptor stimulation (results summarized in Figures 3b and 3c, respectively). Considering that the parasympathetic and sympathetic systems rarely act in isolation, physiological fluid secretion was replicated using a combination of IPR plus CCh. Figure 4a shows that the kinetics in response to IPR plus CCh were essentially identical for *Slc4a7*$^{-/-}$ and *Slc4a7*$^{+/+}$ mice. Moreover, the total amount of saliva generated by physiological-like stimulation was not significantly different between *Slc4a7*$^{+/+}$ and *Slc4a7*$^{-/-}$ mice (results summarized in Figure 4b). Taken together, these results demonstrate that Slc4a7 contributes little to fluid secretion by the SMG under different physiological conditions. Of note, disruption of *Slc4a7* had no significant impact on the amount of saliva secreted by either sex. Consequently, Figures 3 and 4 display pooled results from male and female submandibular glands. A summary of the results from Figures 3 and 4 are given by sex in Table 1.

3.3 HCO_3^- concentration of saliva during β-adrenergic and cholinergic receptor stimulation

Salivary glands secrete HCO_3^-, producing especially high concentrations in response to β-adrenergic stimulation (Young et al., 1970). To explore whether the apical Na^+-HCO_3^- cotransporter Slc4a7 in the SMG ducts is involved in ion secretion, we measured the saliva HCO_3^- concentration stimulated by β-adrenergic and/or cholinergic receptor activation. Figure 5 shows that the average saliva HCO_3^- concentration stimulated by IPR was nearly 90 mM in both *Slc4a7*$^{+/+}$ and *Slc4a7*$^{-/-}$ mice. In contrast, the saliva [HCO_3^-] was about 20 mM when the glands of *Slc4a7*$^{+/+}$ and *Slc4a7*$^{-/-}$ mice were stimulated by CCh or by IPR plus CCh (Figure 5). These results demonstrate that β-adrenergic stimulation induced a 4–5 fold higher HCO_3^- concentration in saliva than did cholinergic stimulation. Moreover,

the K^+ concentration and the magnitude of Na^+ and Cl^- reabsorption in the saliva of *Slc4a7*$^{+/+}$ and *Slc4a7*$^{-/-}$ mice were essentially identical under the three different stimulation conditions, and only subtle differences were seen between female *Slc4a7*$^{+/+}$ and *Slc4a7*$^{-/-}$ mice (summarized in Table 1 by sex). Similar to the HCO_3^- concentration, the average K^+ concentration of the saliva stimulated by IPR was nearly 3-fold greater than that secreted under the other two stimulation conditions in both *Slc4a7*$^{+/+}$ and *Slc4a7*$^{-/-}$ mice, suggesting that both HCO_3^- and K^+ secretion are independent of the Na^+-HCO_3^- cotransporter Slc4a7. Note that the above results do not support the 2-stage saliva secretion model that was based on a study of human female parotid glands (Thaysen, Thorn, & Schwartz, 1954). In contrast to the above results, the Thaysen et al. secretion model predicts that the [K^+] and [HCO_3^-] are independent of flow rate at flow rates greater than 1.0 ml/min but the [K^+] increases at lower salivary flow rates while the [HCO_3^-] decreases. Taken together, *Slc4a7* disruption had little effect on HCO_3^- and K^+ secretion or Na^+ and Cl^- reabsorption by the SMG under β-adrenergic, cholinergic or physiological stimulation.

3.4 Slc4a7 mediates Na^+-HCO_3^- cotransport in CHO-K1 cells

Slc4a7 acts as a Na^+-HCO_3^- cotransporter (NBC) in mouse vascular smooth muscle cells (Boedtkjer et al., 2006). To characterize the NBC-like activity of mouse Slc4a7, CHO-K1 cells transfected with a full-length *Slc4a7* clone were loaded with the pH sensitive fluorescent dye BCECF and then the Na^+-dependent alkalinization monitored in Na^+-depleted cells (see Materials and Methods). Note that transcriptional profiling indicated that all *Slc4a7* exons are expressed in mouse SMG (Gao, Oei, Ovitt, Sincan, & Melvin, 2018). To isolate the NBC-like activity, Cl^- free solutions were used to block Cl^--HCO_3^- exchange, while Na^+/H^+ exchanger activity was inhibited with 10 μM ethyl-isopropyl amiloride (EIPA). Under these conditions, *Slc4a7* transfected CHO-K1 cells displayed a robust intracellular pH increase when the bath perfusate was switched from a Na^+ free to a 145 mM Na^+ containing solution (Figure 6a, black circles), while an alkalinization was absent in empty vector-transfected CHO-K1 cells (white circles). A summary of the alkalinization rates from experiments like those shown in Figure 6a are given in Figure 6b. While most Na^+-HCO_3^- cotransporters are sensitive to DIDS (4,4'-Diisothiocyano-2,2'-stilbenedisulfonic acid) (Romero et al., 2013), human SLC4A7 (Park et al., 2002) and rat Slc4a7 (Choi et al., 2000) are relatively insensitive to 500 μM DIDS, while it is sensitive to the *N*-cyanosulphonamide S0859 (2-Chloro-N-[[2′-[(cyanoamino)sulfonyl][1,1′-biphenyl]-4-yl]methyl]-N-[(4-methylphenyl)methyl]-benzamide), a compound structurally unrelated to DIDS that inhibits Na^+-HCO_3^- cotransport of different species (Ch'en, Villafuerte, Swietach, Cobden, & Vaughan-Jones, 2008). Figure 6b shows that both 100 μM DIDS and 100 μM S0859 completely inhibited the Na^+ dependent, Slc4a7 activity, but it was insensitive to 200 μM EIPA (200 μM EIPA results are given in the Figure 6 legend). Moreover, the Slc4a7-mediated Na^+-HCO_3^- cotransport activity was eliminated under HCO_3^- free conditions (Figure 6b). In summary, mouse Slc4a7 promotes Na^+-HCO_3^- cotransport activity that is fully blocked by a relatively low DIDS concentration. The unique DIDS sensitivity of mouse Slc4a7, along with its S0859 sensitivity and HCO_3^- dependence, were subsequently used below to characterize the NBC-like activity of native SMG duct cells.

3.5 *Slc4a7* disruption does not affect pH_i regulation in mouse SMG duct cells

The above results demonstrated that Slc4a7 targets to the apical membrane of SMG duct cells but appears to contribute little if any to the secretion of HCO_3^-. However, the absence of detectible Slc4a7-mediated HCO_3^- secretion does not exclude the possibility that Slc4a7 regulates the intracellular pH of SMG duct cells. To better understand the role of Slc4a7 in the regulation of intracellular pH, the Na^+-dependent intracellular alkalinization following an acid load was monitored in SMG duct cells loaded with BCECF. Unexpectedly, we found that the Na^+ dependent alkalinization rate was not different between the duct cells isolated from *Slc4a7*$^{+/+}$ and *Slc4a7*$^{-/-}$ mice (Figure 7a). A summary of the alkalinization rates for data from experiments like those shown in Figure 7a are given in Figure 7b. In contrast to the complete block of mouse Slc4a7 activity in CHO-K1 cells in the absence of HCO_3^- and by DIDS or S0859 (Figure 6), Figure 7b shows that the Na^+ dependent alkalinization in SMG duct cells from both *Slc4a7*$^{+/+}$ and *Slc4a7*$^{-/-}$ mice displayed only a modest dependence on extracellular HCO_3^- (~30% decrease in activity) and was relatively insensitive to 100 μM S0859 (30–35% inhibition) as well as 100 μM DIDS (40–55% inhibition) and μM 500 DIDS (35–50% inhibition, 500 μM DIDS results are given in the Figure 7 legend). Given that Slc4a7 was not detectable in acinar cells by immunohistofluorescence (Figure 2), it was not surprising that SMG acinar cells were similarly insensitive to the above conditions (data not shown). Of note, the magnitude of the Na^+ dependent alkalinization, HCO_3^- dependence and sensitivity to inhibitors were not significantly different between SMG duct cells from *Slc4a7*$^{+/+}$ and *Slc4a7*$^{-/-}$ mice.

Taken together, it appears that most of the intracellular pH regulation in SMG duct cells primarily occurs by an unknown Na^+ dependent transport mechanism that is DIDS and S0859 insensitive as well as independent of HCO_3^-. These results suggest that the apical Slc4a7 does not promote Na^+-HCO_3^- cotransport nor contribute significantly to intracellular pH regulation in SMG duct cells. Alternatively, compensation by other potential pH regulation and/or HCO_3^- transport mechanisms may have occurred in the SMG of *Slc4a7*$^{-/-}$ mice. To address this issue, qPCR was performed for other members of the *Slc4* family of HCO_3^- transporters, *Cftr*, and the *Slc9* Na^+/H^+ exchangers (*a1, a2* and *a3*) (Figure 7c). However, there were no differences in the mRNA expression of these genes. The simplest interpretation of these findings is that compensation did likely not occur in the SMG of *Slc4a7*$^{-/-}$ mice, and thus these results are consistent with Slc4a7 not being involved in ductal HCO_3^- secretion. Although mRNA expression levels did not appear to change we cannot rule out the possibility that the functional activities of one or more of these ion transport pathways may have been altered in the SMG of *Slc4a7*$^{-/-}$ mice.

4 DISCUSSION

Salivary gland fluid secretion is driven by the transepithelial movement of anions, i.e. basolateral anion uptake and subsequent efflux across the apical membrane of acinar cells (Lee et al., 2012; Melvin et al., 2005). *Slc4* gene family proteins transport HCO_3^- but their role in this overall process is unclear with exception of the cation-dependent, Cl^--HCO_3^- exchanger Slc4a9 (Pena-Munzenmayer et al., 2015; Vera-Siguenza et al., 2018). Na^+-HCO_3^- cotransporter expression appears to be both salivary gland cell type- and species-specific.

Slc4a7 was reported to be expressed at the luminal membranes of acinar and duct cells in mouse SMG (Luo et al., 2001) and in guinea pig SMG (Li et al., 2006). In contrast, SLC4A7 was localized on the basolateral side of acinar cells and the apical pole of duct cells in human SMG (Namkoong et al., 2015). In the present study, Slc4a7 was localized near the apical membrane of mouse SMG duct cells with no positive staining detected in acinar cells. It is not clear why Slc4a7 was not detected in acinar cells, but one possibility is that Slc4a7 expression may be different in the Black Swiss:129/SvJ hybrid mice used by Luo et al. compared to the 129-Sv/Ev^{Brd} background used in the present study. Regardless, given that the bulk of fluid is secreted by acinar cells (Lee et al., 2012; Melvin et al., 2005), we predicted that the apical Slc4a7 in duct cells would not be involved in fluid secretion in the SMG of 129-Sv/Ev^{Brd} mice. Indeed, the kinetics and magnitude of β-adrenergic and cholinergic induced fluid secretion were essentially identical in wildtype and *Slc4a7* null littermate mice, suggesting that the Slc4a7 Na^+-HCO_3^- cotransporters expressed in the duct cells contribute little if any to fluid secretion in mouse SMG.

It is well established that Slc4a7 regulates intracellular pH (Boedtkjer et al., 2016; Ng et al., 2017) and the current study confirmed that mouse Slc4a7 cotransporter expressed in CHO-K1 cells mediates Na^+ and HCO_3^- dependent regulation of the intracellular pH. In contrast to human SLC4A7 and rat Slc4a7, which are only weakly inhibited by DIDS (Aalkjaer, Boedtkjer, Choi, & Lee, 2014; Choi et al., 2000; Park et al., 2002), the NBC-like activity of mouse Slc4a7 was abolished by 100 μM DIDS. Consistent with mouse Slc4a7 being DIDS-sensitive, Na^+-dependent bicarbonate transport is largely inhibited by 200 μM DIDS in mouse small arteries (Boedtkjer et al., 2006). In contrast, the intracellular pH recovery mediated by NBC-like activity in the human SMG was completely inhibited by DIDS (Namkoong et al., 2015), suggesting that SLC4A7 was not likely involved but another HCO_3^- transporter with NBC-like activity. Thus, the sensitivity of Slc4a7 to DIDS is species specific.

The current salivary gland secretion model predicts that HCO_3^- is secreted as saliva passes through the ducts (Lee et al., 2012; Melvin et al., 2005) where HCO_3^- exits across the luminal membrane (Hong et al., 2014). In the pancreatic duct, functional coupling of the Cl^- channel Cftr and the $Cl^-/HCO3^-$ exchanger Slc26a6 appears to provide the major route for HCO_3^- secretion (Ishiguro et al., 2009; Lee et al., 2012; Y. Wang et al., 2006). However, it was recently shown that Slc26a6 is primarily expressed at the apical membrane of acinar cells in the mouse SMG where it does not contribute to HCO_3^- secretion (Mukaibo, Munemasa, George, et al., 2018). Although Cftr is clearly involved in HCO_3^- secretion by mouse salivary gland ducts (Catalan et al., 2011), the mechanism of HCO_3^- secretion remains to be fully defined. It has been proposed that Slc4a7 functions as a HCO_3^- salvage mechanism during the resting state in mouse salivary gland ducts (Luo et al., 2001). However, the HCO_3^- concentration of the saliva generated by *Slc4a7* null mice was unchanged, even in response to β-adrenergic stimulation when saliva can contain as much as 140 mM HCO_3^- (Young et al., 1970). Of note, enhanced expression of other potential pH regulation and HCO_3^- transport mechanisms (e.g. other members of the Slc4 HCO_3^- transporter family, Cftr anion channel, and Na^+/H^+ exchangers Slc9a1, Slc9a2 and Slc9a3) did not appear to compensate for loss of Slc4a7, consistent with Slc4a7 not being involved in ductal HCO_3^- secretion in the mouse SMG. Similarly, Slc4a7 appears not to

be involved in pH regulation in guinea pig parotid and SMG acinar and duct cells (Li et al., 2006). Given that our results and those of others demonstrate that Slc4a7 is expressed in salivary gland duct cells, why does disruption of Slc4a7 expression fail to affect SMG function? One possibility is that other HCO_3^- transport mechanisms overwhelm Slc4a7 activity in SMG duct cells. Indeed, our qPCR results revealed that Slc4a7 expression was less than half (18.7 units) in wildtype SMG compared to that found for Slc9a1 and Cftr (49.9 and 49.0 units, respectively. These results are consistent with the results of a previous transcriptional expression study (Gao et al., 2018) where Slc9a1 (Nhe1) and Cftr were more highly expressed than Slc4a7 in mouse SMG (Slc4a7 = 0.9, Slc9a1 = 4.1 and Cftr = 2.0 FPKM units, respectively). Alternatively, mouse SMG may express an unknown signaling molecule and/or a regulatory subunit that inhibits Slc4a7 activity under the experimental conditions in the present study.

In summary, the Na^+-HCO_3^- cotransporter Slc4a7 is localized to the apical membrane of mouse SMG duct cells, with no detectable expression in acinar cells. The results of *ex vivo* saliva collection studies reveal that Slc4a7 contributes little to fluid secretion or HCO_3^- secretion under β-adrenergic, cholinergic or physiological-like stimulation. Moreover, Slc4a7 did not appear to promote Na^+-HCO_3^- cotransport in SMG duct cells, indicating that it plays a limited, if any, role in the regulation of intracellular pH.

ACKNOWLEDGEMENTS

J.E. Melvin is the guarantor of this work, had full access to all the data, and takes full responsibility for the integrity of data and the accuracy of data analysis. The authors wish to thank Drs. Marcelo Catalán and Gaspar Peña-Münzenmayer for helpful discussions when this study was conceived and Yasna Jaramillo and Jaideep Honavar for technical assistance. This study was supported by the Intramural Research Program of the National Institute of Dental and Craniofacial Research (NIDCR), NIH (JEM, 1-ZIA-DE000738) and the NIDCR Veterinary Research Core (1-ZIC-DE000740). I. Kurtz is supported in part by NIH DK077162, the Allan Smidt Charitable Fund, and the Factor Family Foundation.

Funding information

Intramural Research Program of the National Institute of Dental and Craniofacial Research (NIDCR), National Institutes of Health (NIH), Grant/Award Numbers:1-ZIA-DE000738; NIDCR Veterinary Research Core, Grant/Award Numbers: 1-ZIC-DE000740; NIH Grants, Grant/Award Numbers: DK077162; the Allan Smidt Charitable Fund, and the Factor Family Foundation.

REFERENCES

Aalkjaer C, Boedtkjer E, Choi I, & Lee S (2014). Cation-coupled bicarbonate transporters. Compr Physiol, 4(4), 1605–1637. doi:10.1002/cphy.c130005 [PubMed: 25428855]

Boedtkjer E, & Aalkjaer C (2012). Intracellular pH in the resistance vasculature: regulation and functional implications. J Vasc Res, 49(6), 479–496. doi:10.1159/000341235 [PubMed: 22907294]

Boedtkjer E, Bentzon JF, Dam VS, & Aalkjaer C (2016). Na+, HCO3--cotransporter NBCn1 increases pHi gradients, filopodia, and migration of smooth muscle cells and promotes arterial remodelling. Cardiovasc Res, 111(3), 227–239. doi:10.1093/cvr/cvw079 [PubMed: 27076468]

Boedtkjer E, Praetorius J, & Aalkjaer C (2006). NBCn1 (slc4a7) mediates the Na+-dependent bicarbonate transport important for regulation of intracellular pH in mouse vascular smooth muscle cells. Circ Res, 98(4), 515–523. doi:10.1161/01.RES.0000204750.04971.76 [PubMed: 16439691]

Boedtkjer E, Praetorius J, Fuchtbauer EM, & Aalkjaer C (2008). Antibody-independent localization of the electroneutral Na+-HCO3- cotransporter NBCn1 (slc4a7) in mice. Am J Physiol Cell Physiol, 294(2), C591–603. doi:10.1152/ajpcell.00281.2007 [PubMed: 18077606]

Boedtkjer E, Praetorius J, Matchkov VV, Stankevicius E, Mogensen S, Fuchtbauer AC, Aalkjaer C (2011). Disruption of Na+,HCO(3)(−) cotransporter NBCn1 (slc4a7) inhibits NO-mediated vasorelaxation, smooth muscle Ca(2)(+) sensitivity, and hypertension development in mice. Circulation, 124(17), 1819–1829. doi:10.1161/CIRCULATIONAHA.110.015974 [PubMed: 21947296]

Bok D, Galbraith G, Lopez I, Woodruff M, Nusinowitz S, BeltrandelRio H, … Kurtz I (2003). Blindness and auditory impairment caused by loss of the sodium bicarbonate cotransporter NBC3. Nat Genet, 34(3), 313–319. doi:10.1038/ng1176 [PubMed: 12808454]

Catalan MA, Scott-Anne K, Klein MI, Koo H, Bowen WH, & Melvin JE (2011). Elevated incidence of dental caries in a mouse model of cystic fibrosis. PLoS One, 6(1), e16549. doi:10.1371/journal.pone.0016549 [PubMed: 21304986]

Ch'en FF, Villafuerte FC, Swietach P, Cobden PM, & Vaughan-Jones RD (2008). S0859, an N-cyanosulphonamide inhibitor of sodium-bicarbonate cotransport in the heart. Br J Pharmacol, 153(5), 972–982. doi:10.1038/sj.bjp.0707667 [PubMed: 18204485]

Choi I (2012). SLC4A transporters. Curr Top Membr, 70, 77–103. doi:10.1016/B978-0-12-394316-3.00003-X [PubMed: 23177984]

Choi I, Aalkjaer C, Boulpaep EL, & Boron WF (2000). An electroneutral sodium/bicarbonate cotransporter NBCn1 and associated sodium channel. Nature, 405(6786), 571–575. doi:10.1038/35014615 [PubMed: 10850716]

Damkier HH, Nielsen S, & Praetorius J (2006). An anti-NH2-terminal antibody localizes NBCn1 to heart endothelia and skeletal and vascular smooth muscle cells. Am J Physiol Heart Circ Physiol, 290(1), H172–180. doi:10.1152/ajpheart.00713.2005 [PubMed: 16126812]

Gao X, Oei MS, Ovitt CE, Sincan M, & Melvin JE (2018). Transcriptional profiling reveals gland-specific differential expression in the three major salivary glands of the adult mouse. Physiol Genomics, 50(4), 263–271. doi:10.1152/physiolgenomics.00124.2017 [PubMed: 29373073]

Gorbatenko A, Olesen CW, Boedtkjer E, & Pedersen SF (2014). Regulation and roles of bicarbonate transporters in cancer. Front Physiol, 5, 130. doi:10.3389/fphys.2014.00130 [PubMed: 24795638]

Gresz V, Kwon TH, Vorum H, Zelles T, Kurtz I, Steward MC, Nielsen S (2002). Immunolocalization of electroneutral Na(+)-HCO cotransporters in human and rat salivary glands. Am J Physiol Gastrointest Liver Physiol, 283(2), G473–480. doi:10.1152/ajpgi.00421.2001 [PubMed: 12121896]

Hong JH, Park S, Shcheynikov N, & Muallem S (2014). Mechanism and synergism in epithelial fluid and electrolyte secretion. Pflugers Arch, 466(8), 1487–1499. doi:10.1007/s00424-013-1390-1 [PubMed: 24240699]

Ishiguro H, Steward MC, Lindsay AR, & Case RM (1996). Accumulation of intracellular HCO3- by Na(+)-HCO3- cotransport in interlobular ducts from guinea-pig pancreas. J Physiol, 495 (Pt 1), 169–178. [PubMed: 8866360]

Ishiguro H, Steward MC, Naruse S, Ko SB, Goto H, Case RM, Yamamoto A (2009). CFTR functions as a bicarbonate channel in pancreatic duct cells. Journal of General Physiology, 133(3), 315–326. doi:10.1085/jgp.200810122 [PubMed: 19204187]

Kao L, Azimov R, Shao XM, Frausto RF, Abuladze N, Newman D, Kurtz I (2016). Multifunctional ion transport properties of human SLC4A11: comparison of the SLC4A11-B and SLC4A11-C variants. Am J Physiol Cell Physiol, 311(5), C820–C830. doi:10.1152/ajpcell.00233.2016 [PubMed: 27581649]

Kwon TH, Pushkin A, Abuladze N, Nielsen S, & Kurtz I (2000). Immunoelectron microscopic localization of NBC3 sodium-bicarbonate cotransporter in rat kidney. Am J Physiol Renal Physiol, 278(2), F327–336. doi:10.1152/ajprenal.2000.278.2.F327 [PubMed: 10662737]

Lau KR, Howorth AJ, & Case RM (1990). The effects of bumetanide, amiloride and Ba2+ on fluid and electrolyte secretion in rabbit salivary gland. J Physiol, 425, 407–427. [PubMed: 2213584]

Lee MG, Ohana E, Park HW, Yang D, & Muallem S (2012). Molecular mechanism of pancreatic and salivary gland fluid and HCO3 secretion. Physiol Rev, 92(1), 39–74. doi:10.1152/physrev.00011.2011 [PubMed: 22298651]

Li J, Koo NY, Cho IH, Kwon TH, Choi SY, Lee SJ, Park K (2006). Expression of the Na+-HCO3- cotransporter and its role in pHi regulation in guinea pig salivary glands. Am J

Physiol Gastrointest Liver Physiol, 291(6), G1031–1040. doi:10.1152/ajpgi.00483.2005 [PubMed: 16782694]

Liu Y, Yang J, & Chen LM (2015). Structure and Function of SLC4 Family [Formula: see text] Transporters. Front Physiol, 6, 355. doi:10.3389/fphys.2015.00355 [PubMed: 26648873]

Lu X, Wang L, Lin X, Huang J, Charles Gu C, He M, Gu D (2015). Genome-wide association study in Chinese identifies novel loci for blood pressure and hypertension. Hum Mol Genet, 24(3), 865–874. doi:10.1093/hmg/ddu478 [PubMed: 25249183]

Luo X, Choi JY, Ko SB, Pushkin A, Kurtz I, Ahn W, Muallem S (2001). HCO3- salvage mechanisms in the submandibular gland acinar and duct cells. J Biol Chem, 276(13), 9808–9816. doi:10.1074/jbc.M008548200 [PubMed: 11139574]

Mangos JA, McSherry NR, Nousia-Arvanitakis S, & Irwin K (1973). Secretion and transductal fluxes of ions in exocrine glands of the mouse. Am J Physiol, 225(1), 18–24. doi:10.1152/ajplegacy.1973.225.1.18 [PubMed: 4714400]

Melvin JE, Yule D, Shuttleworth T, & Begenisich T (2005). Regulation of fluid and electrolyte secretion in salivary gland acinar cells. Annu Rev Physiol, 67, 445–469. doi:10.1146/annurev.physiol.67.041703.084745 [PubMed: 15709965]

Mukaibo T, Munemasa T, George AT, Tran DT, Gao X, Herche J, Melvin JE (2018). The apical anion exchanger Slc26a6 promotes oxalate secretion by murine submandibular gland acinar cells. J Biol Chem. doi:10.1074/jbc.RA118.002378

Mukaibo T, Munemasa T, Masaki C, Cui CY, & Melvin JE (2018). Defective NaCl Reabsorption in Salivary Glands of Eda-Null X-LHED Mice. J Dent Res, 22034518782461. doi:10.1177/0022034518782461

Myers EJ, Marshall A, Jennings ML, & Parker MD (2016). Mouse Slc4a11 expressed in Xenopus oocytes is an ideally selective H+/OH- conductance pathway that is stimulated by rises in intracellular and extracellular pH. Am J Physiol Cell Physiol, 311(6), C945–C959. doi:10.1152/ajpcell.00259.2016 [PubMed: 27681179]

Namkoong E, Shin YH, Bae JS, Choi S, Kim M, Kim N, Park K (2015). Role of Sodium Bicarbonate Cotransporters in Intracellular pH Regulation and Their Regulatory Mechanisms in Human Submandibular Glands. PLoS One, 10(9), e0138368. doi:10.1371/journal.pone.0138368 [PubMed: 26375462]

Ng FL, Boedtkjer E, Witkowska K, Ren M, Zhang R, Tucker A, Ye S (2017). Increased NBCn1 expression, Na+/HCO3- co-transport and intracellular pH in human vascular smooth muscle cells with a risk allele for hypertension. Hum Mol Genet, 26(5), 989–1002. doi:10.1093/hmg/ddx015 [PubMed: 28087731]

Nguyen HV, Stuart-Tilley A, Alper SL, & Melvin JE (2004). Cl(−)/HCO(3)(−) exchange is acetazolamide sensitive and activated by a muscarinic receptor-induced [Ca(2+)](i) increase in salivary acinar cells. Am J Physiol Gastrointest Liver Physiol, 286(2), G312–320. doi:10.1152/ajpgi.00158.2003 [PubMed: 12958022]

Park K, Hurley PT, Roussa E, Cooper GJ, Smith CP, Thevenod F, Case RM (2002). Expression of a sodium bicarbonate cotransporter in human parotid salivary glands. Arch Oral Biol, 47(1), 1–9. [PubMed: 11743927]

Parker MD (2018). Mouse models of SLC4-linked disorders of HCO3(−)-transporter dysfunction. Am J Physiol Cell Physiol, 314(5), C569–C588. doi:10.1152/ajpcell.00301.2017 [PubMed: 29384695]

Pena-Munzenmayer G, Catalan MA, Kondo Y, Jaramillo Y, Liu F, Shull GE, & Melvin JE (2015). Ae4 (Slc4a9) Anion Exchanger Drives Cl- Uptake-dependent Fluid Secretion by Mouse Submandibular Gland Acinar Cells. Journal of Biological Chemistry, 290(17), 10677–10688. doi:10.1074/jbc.M114.612895 [PubMed: 25745107]

Pena-Munzenmayer G, George AT, Shull GE, Melvin JE, & Catalan MA (2016). Ae4 (Slc4a9) is an electroneutral monovalent cation-dependent Cl-/HCO3- exchanger. Journal of General Physiology, 147(5), 423–436. doi:10.1085/jgp.201611571 [PubMed: 27114614]

Proctor GB (2016). The physiology of salivary secretion. Periodontol 2000, 70(1), 11–25. doi:10.1111/prd.12116 [PubMed: 26662479]

Pushkin A, Abuladze N, Lee I, Newman D, Hwang J, & Kurtz I (1999). Cloning, tissue distribution, genomic organization, and functional characterization of NBC3, a new member of the sodium bicarbonate cotransporter family. J Biol Chem, 274(23), 16569–16575. [PubMed: 10347222]

Pushkin A, Clark I, Kwon TH, Nielsen S, & Kurtz I (2000). Immunolocalization of NBC3 and NHE3 in the rat epididymis: colocalization of NBC3 and the vacuolar H+-ATPase. J Androl, 21(5), 708–720. [PubMed: 10975418]

Romero MF, Chen AP, Parker MD, & Boron WF (2013). The SLC4 family of bicarbonate (HCO(3)(−)) transporters. Mol Aspects Med, 34(2–3), 159–182. doi:10.1016/j.mam.2012.10.008 [PubMed: 23506864]

Shei W, Liu J, Htoon HM, Aung T, & Vithana EN (2013). Differential expression of the Slc4 bicarbonate transporter family in murine corneal endothelium and cell culture. Mol Vis, 19, 1096–1106. [PubMed: 23734078]

Thaysen JH, Thorn NA, & Schwartz IL (1954). Excretion of sodium, potassium, chloride and carbon dioxide in human parotid saliva. Am J Physiol, 178(1), 155–159. doi:10.1152/ajplegacy.1954.178.1.155 [PubMed: 13180731]

Vera-Siguenza E, Catalan MA, Pena-Munzenmayer G, Melvin JE, & Sneyd J (2018). A Mathematical Model Supports a Key Role for Ae4 (Slc4a9) in Salivary Gland Secretion. Bull Math Biol, 80(2), 255–282. doi:10.1007/s11538-017-0370-6 [PubMed: 29209914]

Vilas GL, Loganathan SK, Liu J, Riau AK, Young JD, Mehta JS, Casey JR (2013). Transmembrane water-flux through SLC4A11: a route defective in genetic corneal diseases. Hum Mol Genet, 22(22), 4579–4590. doi:10.1093/hmg/ddt307 [PubMed: 23813972]

Wang L, Li H, Yang B, Guo L, Han X, Li L, Gu D (2017). The Hypertension Risk Variant Rs820430 Functions as an Enhancer of SLC4A7. Am J Hypertens, 30(2), 202–208. doi:10.1093/ajh/hpw127 [PubMed: 27784683]

Wang Y, Soyombo AA, Shcheynikov N, Zeng W, Dorwart M, Marino CR, … Muallem S (2006). Slc26a6 regulates CFTR activity in vivo to determine pancreatic duct HCO3- secretion: relevance to cystic fibrosis. EMBO J, 25(21), 5049–5057. doi:10.1038/sj.emboj.7601387 [PubMed: 17053783]

Yang C, Gonzalez-Perez V, Mukaibo T, Melvin JE, Xia XM, & Lingle CJ (2017). Knockout of the LRRC26 subunit reveals a primary role of LRRC26-containing BK channels in secretory epithelial cells. Proc Natl Acad Sci U S A, 114(18), E3739–E3747. doi:10.1073/pnas.1703081114 [PubMed: 28416688]

Young JA, Cook DI, Evans LA, & Pirani D (1987). Effects of ion transport inhibition on rat mandibular gland secretion. J Dent Res, 66(2), 531–536. doi:10.1177/00220345870660022401 [PubMed: 2442220]

Young JA, Martin CJ, Asz M, & Weber FD (1970). A microperfusion investigation of bicarbonate secretion by the rat submaxillary gland. The action of a parasumpathomimetic drug on electrolyte transport. Pflugers Arch, 319(3), 185–199. [PubMed: 5529092]

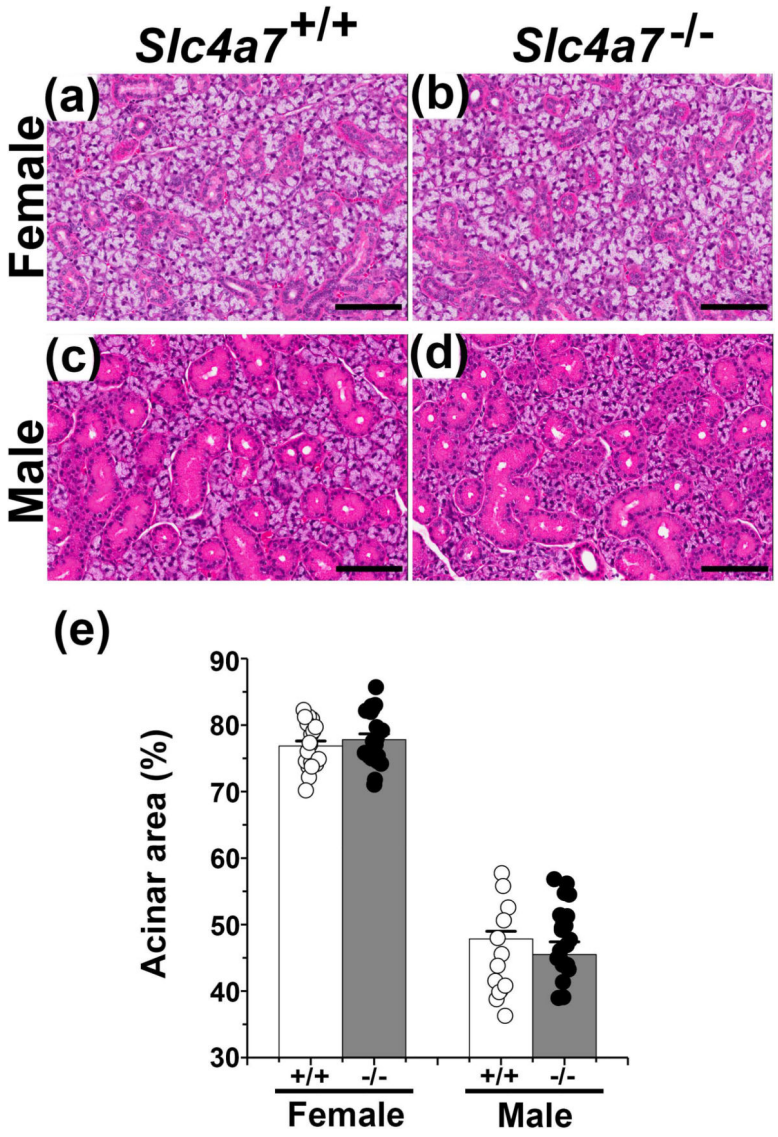

Figure 1.

Histology of submandibular glands (SMG) from wildtype and *Slc4a7* null mice. Five μm thick sections of paraformaldehyde fixed mouse SMG were deparaffinized and stained with hematoxylin-eosin (HE): (a) female $Slc4a7^{+/+}$ SMG, (b) female $Slc4a7^{-/-}$ SMG, (c) male $Slc4a7^{+/+}$ SMG, and (d) male $Slc4a7^{-/-}$ SMG. Black scale bar = 100 μm. (e) The cross-sectional areas of acinar and ductal regions were calculated as described in Materials and Methods and expressed as the % acinar area. Acinar area (%) values are shown for individual glands (circles) along with the mean ± SEM. The cross-sectional areas of acinar and ductal regions were comparable in wildtype mice = 5 (2 males and 3 females) and *Slc4a7* null mice = 6 (3 males and 3 females).

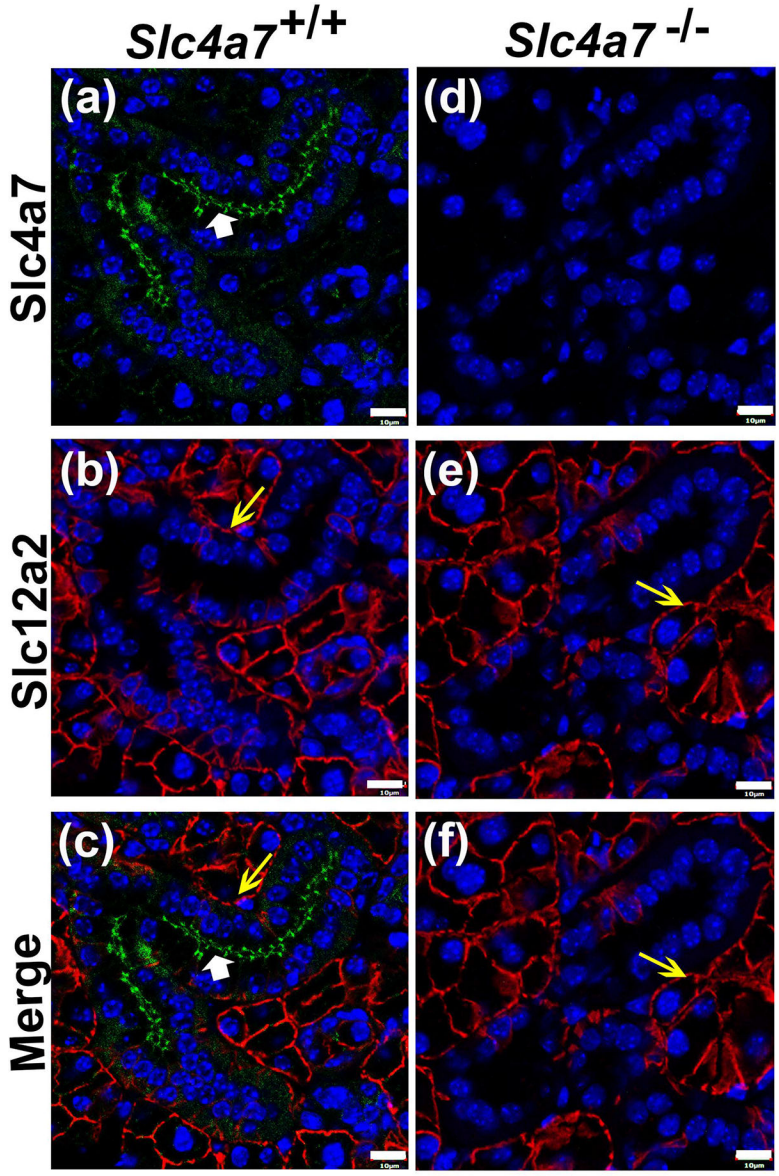

Figure 2.

Immunolocalization of Slc4a7 in the mouse SMG. Immunofluorescence staining of Slc4a7 (green) and Slc12a2/Nkcc1 (red), while nuclei were stained with DAPI (blue). (a) Slc4a7 localized at the apical membrane (white arrowhead) with faint, diffuse intracellular staining in the SMG ducts of *Slc4a7*$^{+/+}$ mice, but no immunostaining was detected in acinar cells. (b) Slc12a2 was labelled at the basolateral membranes of acinar cells from *Slc4a7*$^{+/+}$ mice (yellow arrow). (c) Merged image of Slc4a7 (white arrowhead) and Slc12a2 (yellow arrow) staining in *Slc4a7*$^{+/+}$ mice. (d) Slc4a7-specific immunostaining was not detected in the SMG ducts of the *Slc4a7*$^{-/-}$ mice. (e) Slc12a2 immunostaining was unchanged in *Slc4a7*$^{-/-}$ mice (yellow arrow). (f) Merged image of Slc4a7 and Slc12a2 (yellow arrow) staining from *Slc4a7*$^{-/-}$ mice. White scale bar = 10 μm; immunostaining patterns were comparable in wildtype mice = 5 (2 males and 3 females) and *Slc4a7* null mice = 6 (3 males and 3 females). Images shown are from female *Slc4a7*$^{+/+}$ and *Slc4a7*$^{-/-}$ mice.

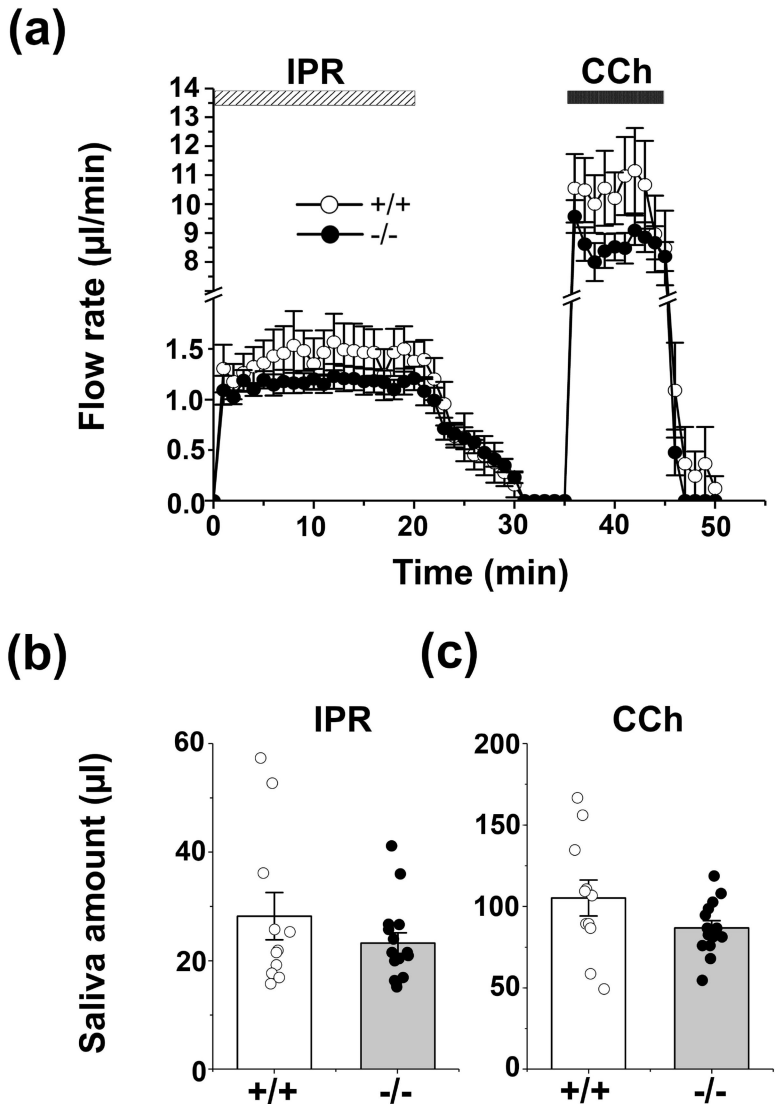

Figure 3.

Flow rate and amount of saliva in response to β-adrenergic vs. cholinergic stimulation of the *ex vivo* SMG. The mouse *ex vivo* SMG was stimulated for 20 min with 1.0 μM IPR, followed by 15 min washout, and finally 10 min perfusion with 0.3 μM CCh in physiological Solution A (Table 2). (a) No differences in the kinetics and rates of salivation (μl/min) were observed in response to 1.0 μM IPR or 0.3 μM CCh, respectively, in the SMG of *Slc4a7*$^{+/+}$ (white circles, n = 11) and *Slc4a7*$^{-/-}$ (black circles, n = 15) mice. (b) The saliva amount (μl) of the *ex vivo* stimulated SMG in response to 1.0 μM IPR, and (c) in response to 0.3μM CCh were comparable in *Slc4a7*$^{+/+}$ (white bars) and *Slc4a7*$^{-/-}$ mice (grey bars). Values are shown for individual glands (circles) along with the mean ± SEM.

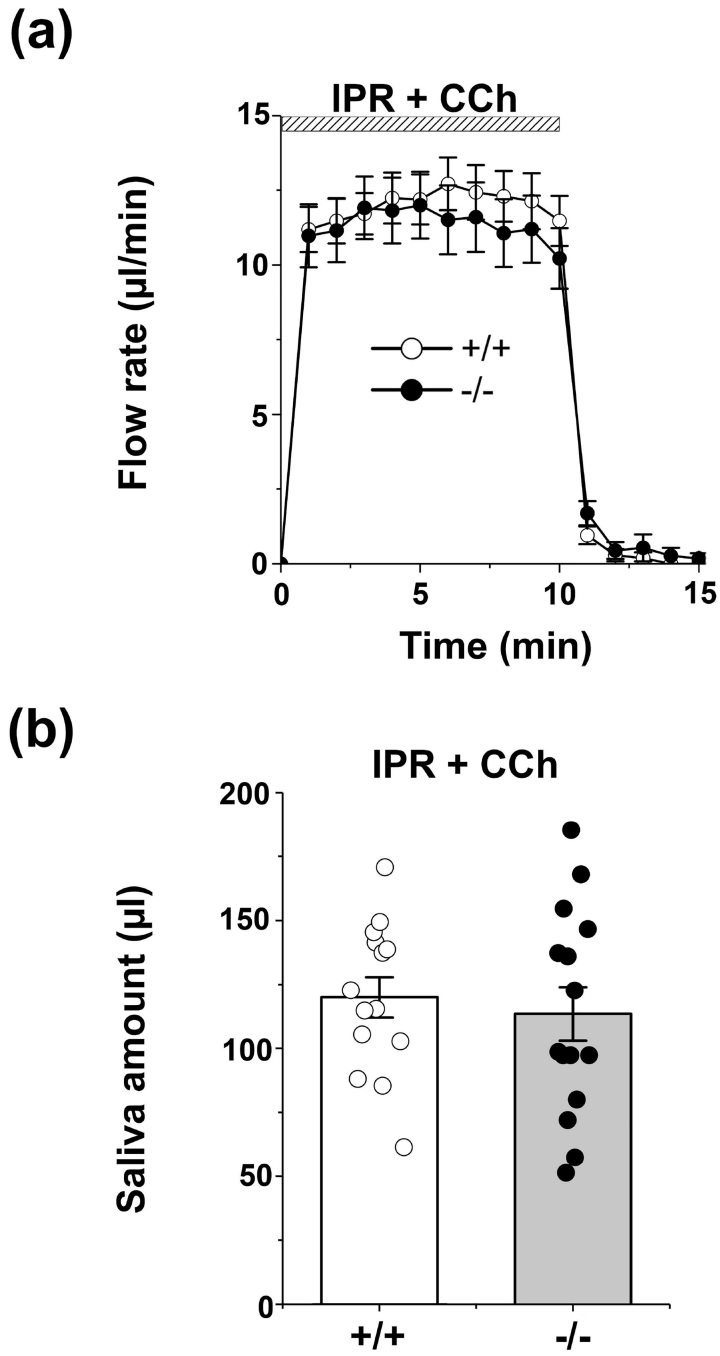

Figure 4.

Flow rate and amount of saliva in response to physiological-like β-adrenergic and cholinergic stimulation of the ex vivo SMG. The mouse *ex vivo* SMG was stimulated for 10 min with the β-adrenergic receptor agonist IPR (1.0 μM) plus the cholinergic receptor agonist CCh (0.3 μM) in physiological Solution A (Table 2). (a) No differences in the kinetics and rates of salivation (μl/min) were observed between *Slc4a7*$^{+/+}$ (white circle, n=14) and *Slc4a7*$^{-/-}$ mice (black circle, n=15). (b) The saliva amount (μl) of the *ex vivo*

stimulated SMG was comparable in *Slc4a7*$^{+/+}$ (white bars) and *Slc4a7*$^{-/-}$ mice (grey bars). Values are shown for individual glands (circles) along with the mean ± SEM.

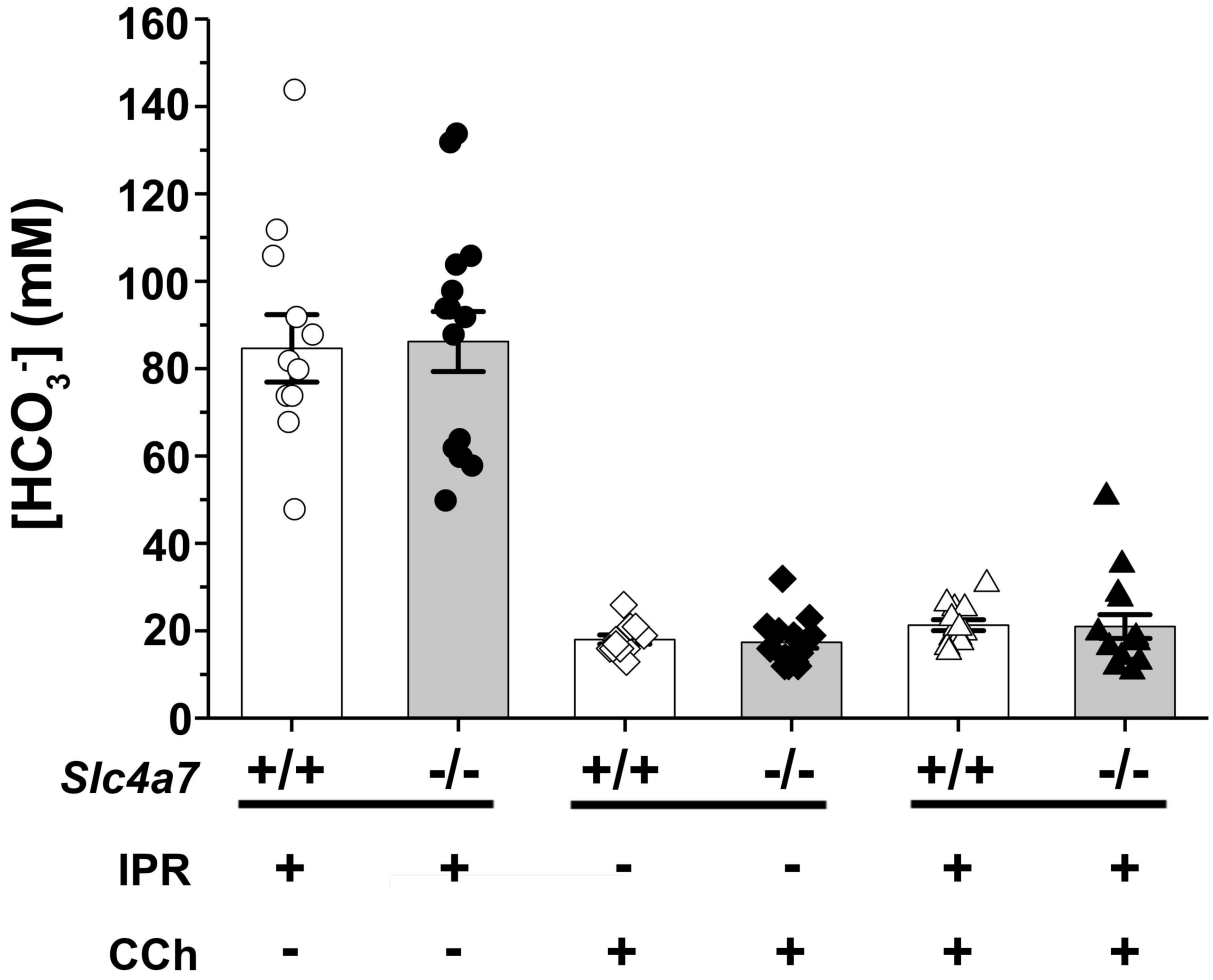

Figure 5.

HCO_3^- concentration of saliva secreted by the *ex vivo* SMG. The HCO_3^- concentrations (mM) in the saliva of the *ex vivo* SMG were comparable in *Slc4a7*$^{+/+}$ (white bars) and *Slc4a7*$^{-/-}$ mice (grey bars). As shown in Figures 3 and 4, salivation was stimulated with 1.0 μM IPR (circles: +/+, n=11; −/−, n=15; far left two bars), 0.3 μM CCh (diamonds: +/+, n=11; −/−, n=15; middle two bars), or 1.0 μM IPR plus 0.3 μM CCh (triangles: +/+, n=14; −/−, n=15; far right two bars). Values are shown for individual glands (symbols) along with the mean ± SEM.

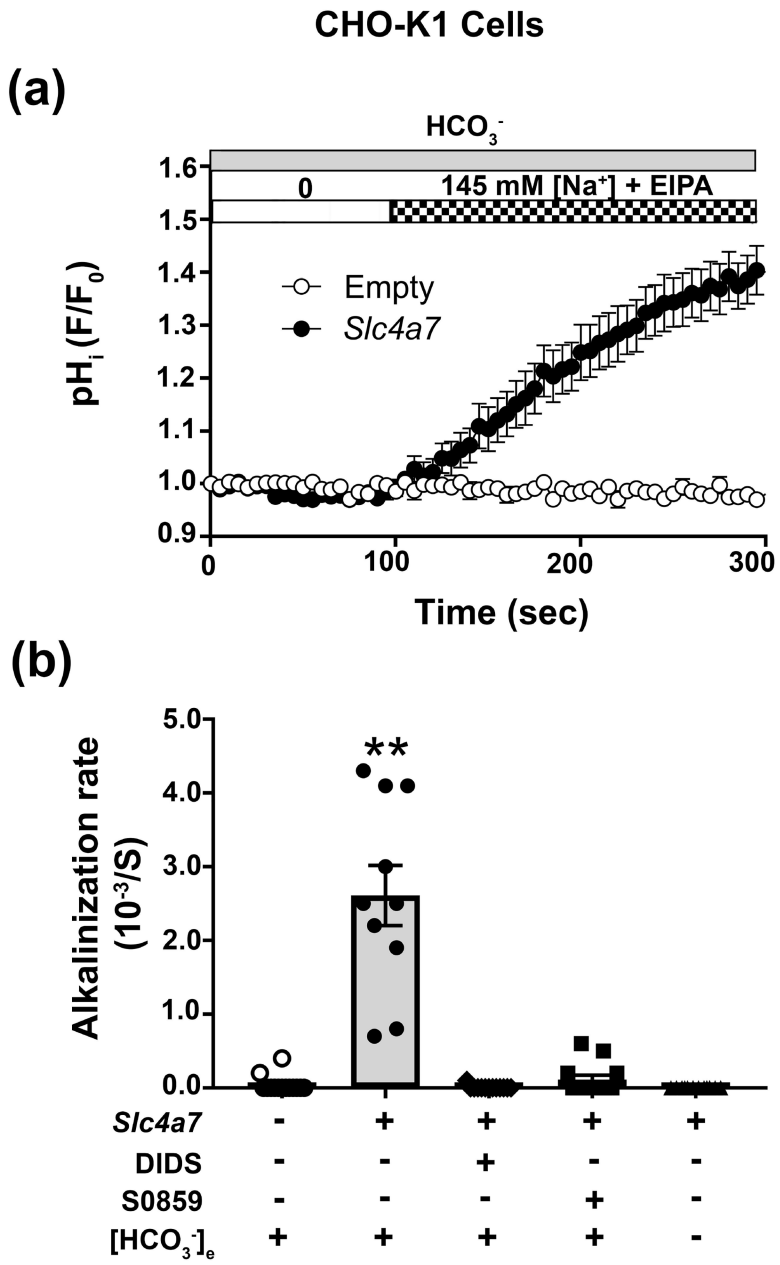

Figure 6.

Mouse *Slc4a7* expression in CHO-K1 cells mediates Na^+-HCO_3^- cotransport. CHO-K1 cells transfected with either the full-length mouse *Slc4a7* cDNA or empty vector were co-transfected with human CD8A cDNA and loaded with the pH sensitive dye BCECF in a K^+ free solution (Solution B, Table 2) containing 0.1 mM of the Na^+-K^+ ATPase inhibitor Ouabain and Dynabeads™ CD8 beads. Extracellular Na^+ was removed for at least 5 min, and then the intracellular alkalinization monitored following re-addition of extracellular Na^+ in BCECF-loaded CHO-K1 cells decorated with CD8 beads. All solutions were Cl^- free and contained 10 μM EIPA to block Cl^-/HCO_3^- and Na^+/H^+ exchange, respectively. (a) A significant increase in the pH_i was observed in *Slc4a7* transfected CHO-K1 cells (black circles, n=10) when switched from Na^+ free to Na^+ containing (Solutions C and B,

respectively, Table 2) HCO_3^- solutions. In contrast, an alkalinization was absent in empty vector transfected CHO-K1 cells (white circles, n=14). (b) Summary of the alkalinization rates for experiments like those shown in panel 6a for CHO-K1 cells transfected with either *Slc4a7* (grey bars) or empty (white bars) vector. The Na^+ dependent, Slc4a7 mediated alkalinization was completely inhibited either by the presence of 100 μM DIDS (4,4'-Diisothiocyano-2,2'-stilbenedisulfonic acid), 100 μM S-0859 (*N*-cyanosulphonamide) or by HCO_3^- free conditions in the presence of the carbonic anhydrase inhibitor ethoxzolamide (EZA, 30 μM), but was insensitive to 200 μM EIPA [results not shown, alkalinization rate (10^{-3}/S): 200 μM EIPA = 2.55 ± 0.49 (n = 11) vs. 10 μM EIPA = 2.61 ± 0.41 (n = 10); $p>0.92$]. Values are shown for the average results (HCO_3^- containing = circles; DIDS = diamonds; S0859 = squares; HCO_3^- free = triangles) along with the mean ± SEM from at least ten different individual transfections. The rate of the Slc4a7 mediated alkalinization in a HCO_3^- containing solution (grey bar, black circles) was significantly greater (**, $p<0.01$) compared to all other conditions.

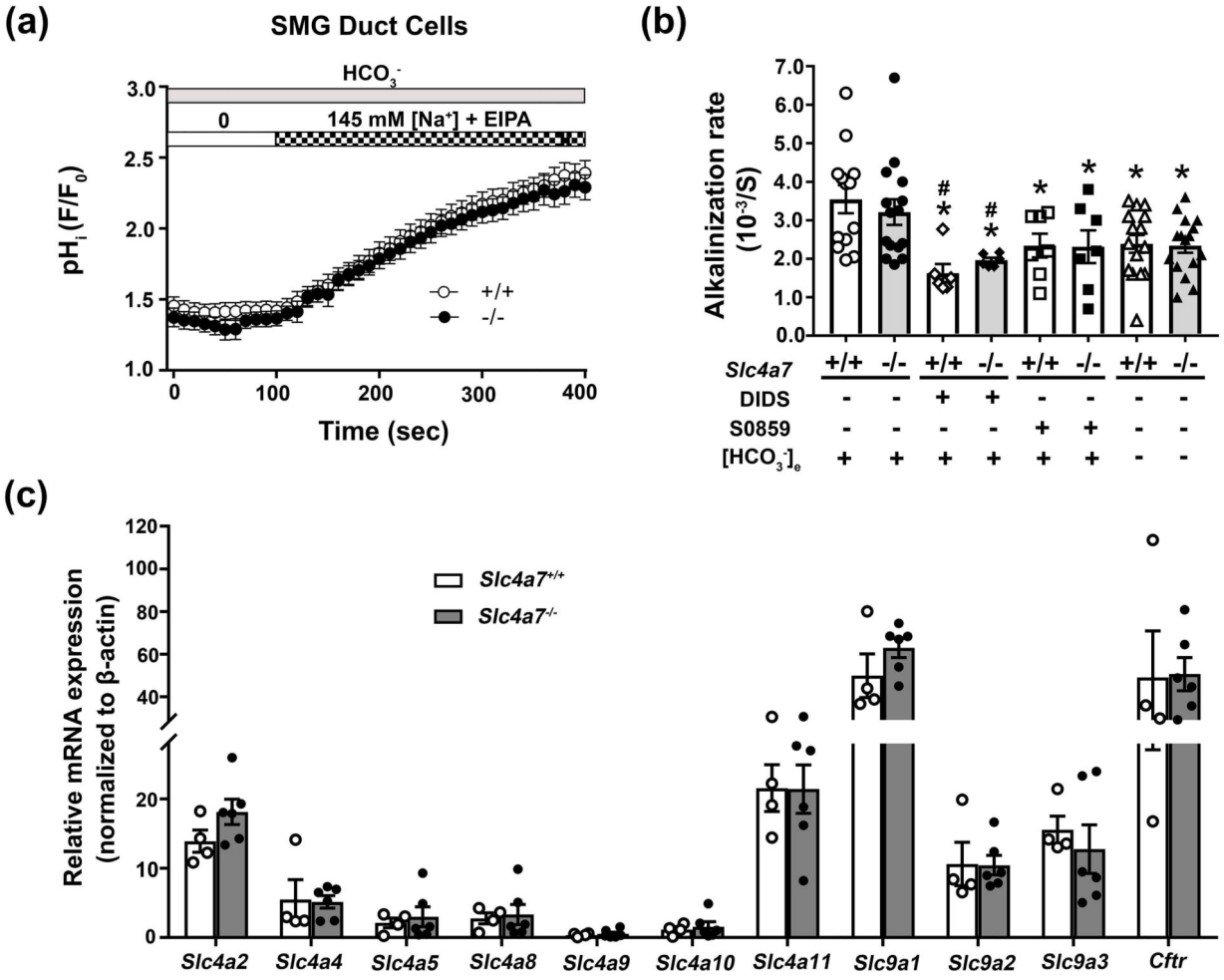

Figure 7.

Slc4a7 disruption fails to affect pH_i regulation in SMG duct cells. Duct cells isolated from *Slc4a7*$^{+/+}$ and *Slc4a7*$^{-/-}$ mouse SMG were loaded with the pH sensitive dye BCECF and the Na^+ dependent intracellular pH (pH_i) recovery monitored following an NH_4^+-prepulse induced intracellular acidosis. All solutions were Cl^- free and contained 10 μM EIPA to block Cl^-/HCO_3^- and Na^+/H^+ exchange, respectively. HCO_3^- containing and HCO_3^- free NH_4^+ solutions were Solutions E and H (Table 2), respectively. (a) The increase in the pH_i observed in duct cells of *Slc4a7*$^{-/-}$ (black circles, n=15) and Slc4a7$^{+/+}$ (white circles, n=13) mice was comparable when switched from Na^+ free to Na^+ containing HCO_3^- solutions (Solutions F and D, respectively, Table 2). (b) Summary of the alkalinization rates for experiments like those shown in panel 7a for SMG duct cells from either *Slc4a7*$^{-/-}$ (grey bars) or *Slc4a7*$^{+/+}$ (white bars) mice. Values are shown for individual mice (HCO_3^- containing = circles; DIDS = diamonds; S0859 = squares; HCO_3^- free = triangles) along with the mean ± SEM of ducts isolated from at least six different mice. The alkalinization rate in a HCO_3^- containing solution for *Slc4a7*$^{+/+}$ mice (white bar, white circles) was significantly greater (*, $p<0.05$) than in the presence of DIDS (white bar, white diamonds). Of note, the Na^+ dependent alkalinization induced in SMG duct cells by switching from Solution F to D (Table 2) was only moderately sensitive to DIDS (100 μM) and S0859

(100 μM) or dependent on HCO_3^- (switching from Na^+ free to Na^+ containing HCO_3^- free solutions, Solution I to G, Table 2, HCO_3^- free in the presence of 30 μM carbonic anhydrase inhibitor EZA) [results not shown for 500 μM DIDS, alkalinization rate (10^{-3}/S): 500 μM DIDS = 1.83 ± 0.40 (n = 7) and 2.12 ± 0.27 (n = 10) for *Slc4a7*$^{+/+}$ and *Slc4a7*$^{-/-}$, respectively; ANOVA test $p>0.66$]. (c) Summary of qPCR results for *Slc4* (*a2, a4, a5, a8, a9, a10* and *a11*), *Slc9* (*a1, a2* and *a3*) and *Cftr*, normalized to *β-actin* expression. Values are shown for individual SMG (white circles = *Slc4a7*$^{+/+}$; black circles = *Slc4a7*$^{-/-}$) along with the mean ± SEM of glands isolated from 4 *Slc4a7*$^{+/+}$ and 6 *Slc4a7*$^{-/-}$ mice. Note break in Y axis for *Slc9a1* and *Cftr*.

Table 1

Characterization of submandibular salivary glands in female and male *Slc4a7*$^{+/+}$ and *Slc4a7*$^{-/-}$ mice

		Female				Male			
		+/+	n	−/−	n	+/+	n	−/−	n
Body weight (g)		20.26 ± 0.63	12	19.83 ± 0.31	16	28.10 ± 0.74	13	27.05 ± 0.57	14
Gland weight (mg)		42.86 ± 1.95	12	39.72 ± 1.56	16	87.72 ± 3.65	13	80.64 ± 1.59	14
Saliva amount (µl) ***[normalized % acini]***	IPR†	19.54 ± 1.83	5	19.83 ± 1.23	8	35.44 ± 6.65	6	27.19 ± 3.33	7
	CCh‡	*[15.01]* 96.27 ± 4.83	5	*[15.43]* 82.5 ± 6.13	8	*[16.13]* 112.67 ± 20.17	6	*[13.02]* 92.67 ± 6.21	7
	IPR+CCh§	*[73.94]* 109.62 ± 13.95	7	*[64.19]* 91.08 ± 11.53	8	*[51.26]* 130.10 ± 6.50	7	*[44.39]* 139.05 ± 12.84	7
		[84.19]		*[70.86]*		*[59.20]*		*[66.60]*	
HCO_3^-concentrtion (mM)	IPR	103.8 ± 9.22	5	82.3 ± 6.59	8	65.47 ± 5.50	6	90.66 ± 13.14	7
	CCh	19.9 ± 1.70	5	17.15 ± 1.42	8	16.4 ± 1.06	6	17.61 ± 2.60	7
	IPR+CCh	20.85 ± 1.56	7	14.97 ± 1.06**	8	21.62 ± 2.01	7	27.81 ± 4.60	7
K^+concentration (mM)	IPR	92.13 ± 6.46	5	93.72 ± 4.25	8	83.80 ± 8.40	6	86.17 ± 6.14	7
	CCh	27.89 ± 0.69	5	31.75 ± 1.11*	8	42.78 ± 2.70	6	40.83 ± 2.01	7
	IPR+CCh	35.05 ± 1.41	7	40.28 ± 1.34*	8	40.73 ± 2.85	7	38.48 ± 3.65	7
Na^+reabsorption (mM)	IPR	135.66 ± 8.11	5	133.48 ± 5.79	8	123.20 ± 10.77	6	123.96 ± 6.93	7
	CCh	138.59 ± 2.57	5	140.79 ± 3.59	8	139.13 ± 7.47	6	141.72 ± 3.95	7
	IPR+CCh	130.83 ± 2.69	7	146.42 ± 3.12**	8	128.10 ± 3.91	7	142.58 ± 5.57	7
Cl^-reabsorption (mM)	IPR	74.31 ± 5.14	5	57.73 ± 5.07	8	59.73 ± 11.04	6	52.96 ± 6.44	7
	CCh	80.29 ± 1.90	5	78.99 ± 2.96	8	60.86 ± 6.50	6	66.84 ± 3.52	7
	IPR+CCh	91.22 ± 2.36	7	93.29 ± 2.86	8	92.49 ± 2.90	7	95.0 ± 4.07	7

Values are mean ± SEM, n represents the number of mice used in each experiment. Superscripts:

†= 20 min stimulation with β-adrenergic receptor agonist isoproterenol (IPR; 1.0 µM);

‡= 10 min perfusion with cholinergic receptor agonist carbachol (CCh; 0.3 µM); and

§=10 min stimulation with 1.0 µM IPR plus 0.3 µM CCh.

Saliva amount was normalized to the % of gland mass representing the secretory acinar compartment (see Figure 1; µl saliva ÷ % acini for female *Slc4a7*$^{+/+}$ and *Slc4a7*$^{-/-}$ SMG = 76.8 and 77.8%, respectively, and male *Slc4a7*$^{+/+}$ and *Slc4a7*$^{-/-}$ SMG = 45.5 and 47.9%, respectively. The normalized % acini data are given brackets.

* $p<0.05$ or

** $p<0.01$, female *Slc4a7*$^{+/+}$ vs. *Slc4a7*$^{-/-}$ mice.

Table 2

Solutions used in *ex vivo* perfusion and intracellular pH imaging experiments

Solutions	A	B	C	D	E	F	G	H	I
KCl	4.3	-	-	-	-	-	-	-	-
NaCl	120	-	-	-	-	-	-	-	-
K-Gluconate	-	-	-	4.3	4.3	4.3	4.3	4.3	4.3
Na-Gluconate	-	128.3	-	120	-	-	145	-	-
NH_4HCO_3	-	-	-	-	25	-	-	-	-
NH4-Gluconate	-	-	-	--	-	-	-	25	-
NMDG	-	-	128.3	-	120	120	-	120	145
D-Glutamate acid	-	-	128.3	-	120	120	-	120	145
Choline-HCO3	-	-	25	-	-	25	-	-	-
NaHCO3	25	25	-	25	-	-	-	-	-
Glucose	5	5	5	5	5	5	5	5	5
HEPES	10	10	10	10	10	10	10	10	10
CaCl2	1	-	-	-	-	-	-	-	-
MgCl2	1	-	-	-	-	-	-	-	-
Ca-Gluconate	-	1	1	1	1	1	1	1	1
Mg-Gluconate	-	1	1	1	1	1	1	1	1
pH	7.2	7.2	7.2	7.2	7.2	7.2	7.4	7.4	7.4
Gassed	5% CO_2/ 95% O_2						100% O_2		

HCO_3^- containing Solution A was used for the *ex vivo* perfusion experiments shown in Figures 3, 4 and 5. Solutions B, C, D, E and F were HCO_3^- containing solution, while HCO_3^- free solutions G, H and I were used for the intracellular pH measurements experiments shown in Figures 6 and 7. Solutions E and H were used to acid load SMG duct cells by the NH_4^-prepulse technique. Unit: mM.

Table 3

Real-time PCR Primer design

gene symbol	Forward	Reverse	Accession number
Slc4a2	GGAGAAGACAAAGGACCTGATAG	GCTACTGCAGAACGAGAAGAA	NM_001253892
Slc4a4	CCAGCAGCAGTATCCTCAAA	CTGTCTCCTTCCATTCCATCTC	NM_001136260
Slc4a5	CACTCACACCCATCGCTATT	GGTCTCCTCCAGTATCCTCTT	NM_001166067
Slc4a8	GGACGATCGAGGATGGTTTATT	GCTTGTGTTCCTTCCTGTTAATG	NM_001347102
Slc4a9	GCTCTACTGCTGTCAATCCTTAT	CTCCCTTCTGCAGTCTGTATTC	NM_001271544
Slc4a10	AGCATCGTTCCTGTTTCTCTAC	ATACGACCTTCAGTTGCTTCTC	NM_001242378
Slc4a11	CCTCCAATCTCTGTGTACTGC	CTTGAAGTATCCCTGAGTGCC	NM_001081162
Slc9a1	CTTTGAGGAATTTGCCAGCTATG	GAGGTAAATCGGGAGGTGAAAG	NM_001358455
Slc9a2	ACCAACCCAAGTCCAGTATTG	GCTTCCTTATTTTCTCTTCACGG	NM_001033289
Slc9a3	TCCCTCTATGGTGTCTTCCTC	CCAAACAGCAAGAAATCCAGG	NM_001081060
Cftr	GCCAAGGCAAGTCCTTCATCA	GCCATTTACCTTGGCATAGGC	NM_021050
β-actin	ACCTTCTACAATGAGCTGCG	CTGGATGGCTACGTACATGG	NM_007393

J Cell Physiol. Author manuscript; available in PMC 2020 August 14.